communications earth & environment

Article

A Nature Portfolio journal

https://doi.org/10.1038/s43247-025-02263-8

Coastal inorganic mercury time series reveals interannual and seasonal variability driven by regional climate factors

Hannah M. Adams [1] ✉, Peipei Wu[1], Iris Kübler-Dudgeon[1], Carl H. Lamborg[2], Jeff S. Bowman[1] & Amina T. Schartup [1] ✉

Inorganic mercury (iHg) is an anthropogenic pollutant that forms monomethylmercury, a neurotoxicant affecting human health through seafood consumption. Despite iHg emissions reductions, the impact on oceanic concentrations remains unclear due to limited long-term data. Here, we present a four-year weekly time series of oceanic iHg concentrations at Scripps Pier in La Jolla, California, capturing interannual and seasonal variability. Interannual variability is driven by wet season precipitation, with wet years exhibiting sevenfold higher iHg concentration variance than dry years, potentially linking to El Niño-Southern Oscillation. Seasonally, precipitation and wave dynamics influence iHg inputs, with wet seasons driven by precipitation and runoff and dry seasons by upwelling. These parameters informed a model built to reconstruct a 20-year record of iHg concentrations, suggesting a long-term decline of 0.005 pM yr^{-1} due to climate-driven effects alone. This study highlights challenges in detecting long-term trends and emphasizes the need for sustained monitoring of oceanic iHg.

Mercury (Hg) is a global pollutant that poses risks to human health through the consumption of seafood containing monomethylmercury (MMHg), a bioaccumulating neurotoxicant[1]. Anthropogenic emissions release inorganic Hg (iHg) as elemental (Hg^0) and divalent (Hg^{II}) forms into the atmosphere and rivers, which are ultimately deposited to the Earth's surface, including the ocean. Precipitation, also referred to as wet deposition[2,3], and river runoff [4,5] primarily supply Hg^{II} and are influenced by both natural and anthropogenic factors, while dry atmospheric deposition delivers Hg^0 primarily from anthropogenic emissions[6]. Once in the ocean, Hg^0 can oxidize to Hg^{II}, which serves as the substrate for MMHg formation[7–9], linking anthropogenic Hg emissions to marine MMHg risks.

Global efforts to reduce iHg emissions, notably through the United Nations Minamata Convention, are currently being evaluated for their effectiveness in decreasing environmental Hg concentrations. To determine the impacts of anthropogenic emissions reduction efforts, it is important to establish long-term oceanic monitoring to distinguish between the influences of anthropogenic emissions, regional physical processes, and climate variability. Understanding the processes driving concentration variability is critical for evaluating the success of policies aimed at reducing iHg and MMHg concentrations in marine ecosystems.

Most oceanographic studies rely on large-scale transects, where discrete sampling stations are occupied at fixed time points. While these studies have been effective for mapping Hg distributions across ocean basins[10–13], the stations are rarely revisited. This results in limited temporal resolution, which makes it difficult to understand how environmental variability impacts biogeochemical processes. Alternatively, regularly sampled time series offer a framework to analyze iHg concentrations over the range of environmental conditions, providing insights into baseline observations, seasonal cycles, and anthropogenic change. Existing Hg time series have focused on atmospheric Hg[14,15] and riverine Hg concentrations and export[5,16,17], which have proved useful in evaluating changes in regional anthropogenic emissions and informing policy actions through the United Nations Minamata Convention. On the other hand, few studies have examined oceanic Hg variability, despite its direct relevance to human exposure through seafood consumption. Global biogeochemical models have been used to evaluate the timeline to observe changes in seawater Hg concentrations[18,19]; however, the response time is unclear and highly dependent on the rate of emissions reductions and climate change impacts on the Hg biogeochemical cycle. Thus, to better understand how emissions reduction policies impact

[1]Scripps Institution of Oceanography, University of California San Diego, La Jolla, CA, USA. [2]Department of Ocean Sciences, University of California Santa Cruz, Santa Cruz, CA, USA. ✉e-mail: hadams@ucsd.edu; aschartup@ucsd.edu

oceanic concentrations, it is essential to establish marine time series to evaluate long-term variability in iHg concentrations.

The California Current System is a highly productive fishery, supplying 110 million pounds of commercial seafood landings in 2023[20]. As a result, monitoring seawater iHg concentrations in this region can help assess the risks of MMHg exposure from local seafood. The Ellen Browning Scripps Memorial Pier (Scripps Pier; Fig. 1) at Scripps Institution of Oceanography in La Jolla, California is a long-term oceanographic monitoring site that is part of a network of sites managed by the Southern California Coastal Ocean Observing System (SCCOOS). Seawater to a maximum depth of 6 m can be sampled here, and existing time series include observations for physical, biological, and chemical parameters, with some dating back to the early 1900s (Supplementary Fig. 1)[21–23]. Due to the abundance of ongoing time series, this area is well-characterized and an ideal location to establish a high-resolution time series of iHg concentrations. By introducing this temporal aspect to our measurements, we can determine the drivers of iHg supply and variability in the water column.

Here, we present four years of weekly iHg measurements from surface waters (≤ 6 m) at Scripps Pier, establishing the first high-resolution time series of oceanic iHg concentrations, to the best of our knowledge. We find that precipitation and wave height are significant positive predictors of iHg concentrations, and we use these parameters to develop a two-component multiple linear regression plus autoregressive moving average model that reconstructs iHg concentrations back to 2004. This modeled historical time series provides insights into the interannual variability of iHg supply and allows us to evaluate the potential impact of climate variability on oceanic iHg concentrations.

Results and Discussion

Observations from 2021 to 2024 reveal that regional processes control interannual variability and seasonal patterns in iHg concentrations

In surface waters (≤ 6 m) at Scripps Pier, iHg concentrations in unfiltered samples remained relatively stable over the study period, with concentrations exhibiting a log normal distribution, averaging 2.64 pM, with a lower standard deviation of 1.83 pM and an upper standard deviation of 2.85 pM ($n = 333$, Fig. 2a). These concentrations align with observations from the broader California Current System[24,25], providing a baseline for evaluating interannual variability, seasonal trends, and short-term influences. While we sampled from both 0.5 m and 6 m depths, we chose to analyze these samples together. This is because the water column depth is shallow and within the mixed layer, and differences between the two sampling depths can be attributed to slight differences in biogeochemical processes influencing the waters. The 6 m samples may be more influenced by interactions with deeper water masses and sediments[26–28], whereas the 0.5 m samples are likely more impacted by air-sea exchange processes[29]. Throughout the sampling period, 95% of samples at both depths remain below 2 pM, while notable spikes exceeding 2 pM were observed during precipitation events and periods of increased wave height, highlighting the major factors controlling iHg in these waters (Fig. 2a–c).

Interannual variability in marine iHg concentrations was observed throughout the sampling period, which we attribute to California's highly variable wet season precipitation. The wet season, spanning October to March, is characterized by the largest year-to-year variability in the continental United States[30]. Based on precipitation anomalies since 1940 at

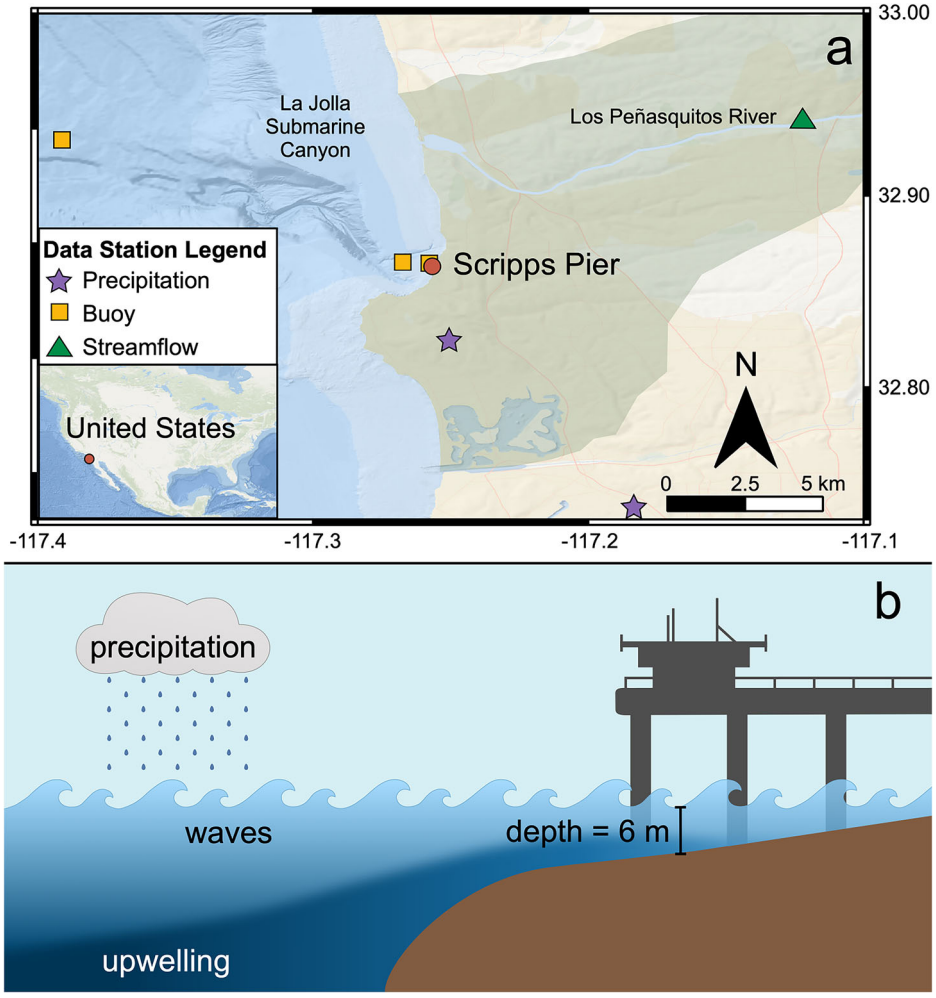

Fig. 1 | Location of Scripps Pier and environmental processes that impact inorganic mercury concentrations at Scripps Pier. a Map of Scripps Pier (red circle) in La Jolla, California with the location of monitoring sites for precipitation (purple star), buoys (yellow square), and streamflow (green triangle). General locations for the La Jolla Submarine Canyon and Los Peñasquitos River are labeled, and the shaded green area represents the watershed region for the Los Peñasquitos River. Currents in the region are seasonally influenced, but generally, there is a poleward-flowing coastal current[75,76], and during precipitation events, river plume waters flow southward from the Los Peñasquitos River outflow[43]. Map created using QGIS. **b** Schematic of environmental processes that impact inorganic mercury concentrations at Scripps Pier, including precipitation, waves, and upwelling. The maximum depth that can be sampled from Scripps Pier is 6 m.

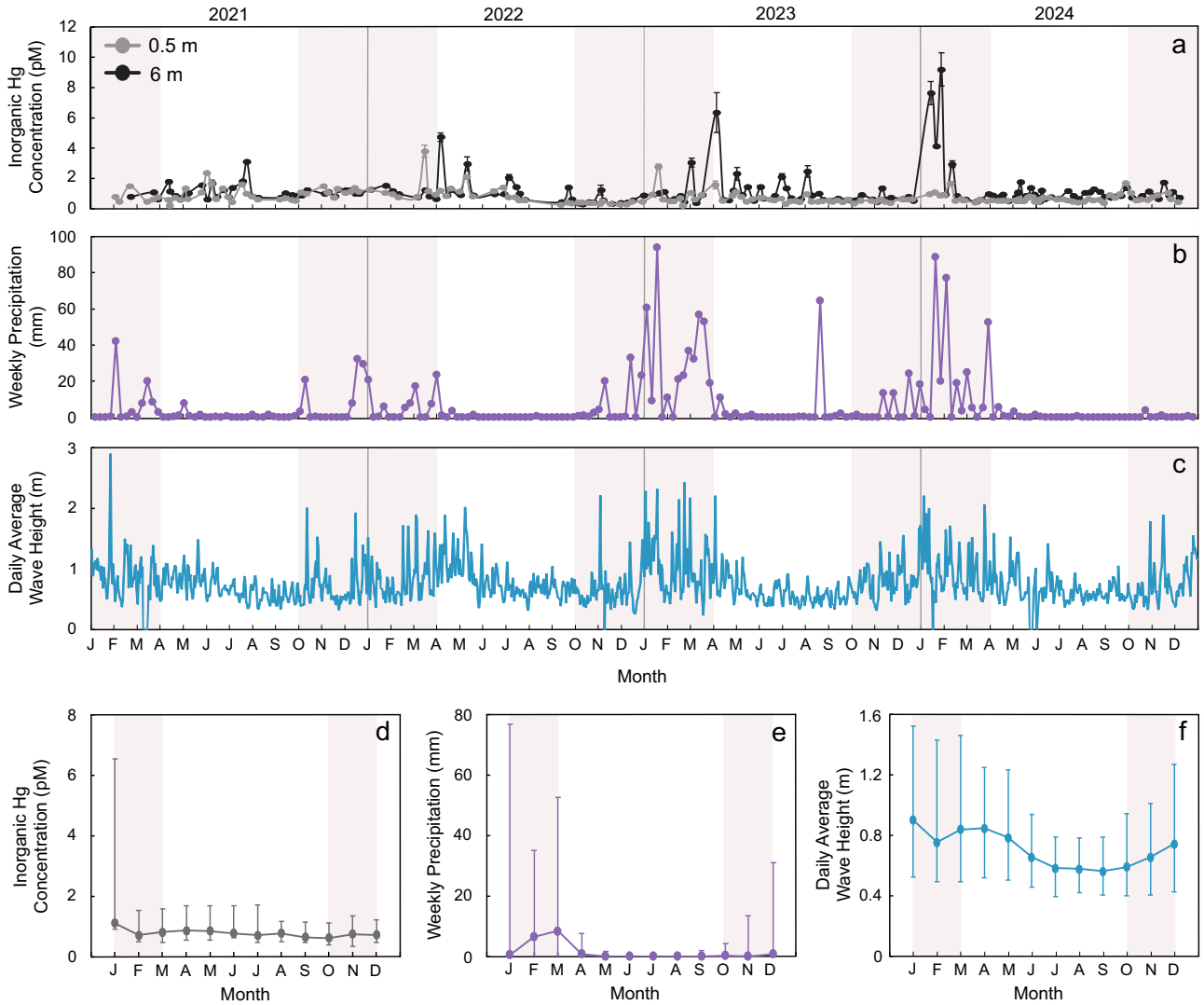

Fig. 2 | Time series of inorganic mercury (Hg) concentrations, precipitation, and wave height at Scripps Pier between 2021-2024. Pink shading indicates the wet season between October to March, and unshaded (white) background indicates the dry season between April to September. **a** Weekly samples of inorganic Hg concentrations were taken at 0.5 m and 6 m depth. Error bars represent the standard deviation of replicate measurements. **b** Weekly sum of precipitation from Station USW00023188 located 16 km away from Scripps Pier[31] (Supplementary Fig. 2), we classified each year's wet season as either "wet" or "dry." During the dry conditions in 2021 (111 mm of rain) and 2022 (154 mm), elevated (>2 pM) iHg concentrations occurred infrequently. In contrast, during the wet conditions in 2023 (346 mm) and 2024 (309 mm), iHg concentrations exhibited seven times larger variance than during dry conditions in 2021 and 2022 (F-test, $p = 5.5 \times 10^{-10}$, $n_{wet} = 43$, $n_{dry} = 85$; Supplementary Fig. 3). These findings reveal that interannual variability in wet season rainfall significantly influences oceanic iHg concentrations during the sampling period. This relationship is likely driven by multiple biogeochemical processes. Increased precipitation directly delivers atmospheric iHg to surface waters[2,3,32–34] and subsequent runoff from rivers[4,5,35] carries terrestrial and sediment-bound iHg into the coastal ocean, which contribute to elevated unfiltered concentrations of iHg in the water column. Additionally, increased wind speeds during rainfall events induce water column mixing that can resuspend iHg from the sediments[36], transporting iHg to the water column. With more precipitation events during the wet season, this allows for more inputs of iHg into the surface waters at Scripps Pier. These findings reveal that interannual variability in wet season rainfall significantly influences oceanic iHg concentrations during this study period by modulating these physical and biogeochemical pathways.

Given the relationship between wet season precipitation and surface water iHg concentrations, we explored the link between broader climatic factors that influence rainfall patterns and the impact on iHg dynamics. One climate mode that modulates precipitation and oceanographic conditions in California is El Niño-Southern Oscillation (ENSO; Supplementary Fig. 4). La Niña conditions (negative ENSO anomaly) are associated with dryer winters and increased summer upwelling, while El Niño conditions (positive ENSO anomaly) are associated with wetter winters and decreased summer upwelling[37–39]. During the course of our sampling period, the wet seasons were predominately influenced by La Niña conditions, so we were unable to compare how positive and negative ENSO anomalies impact wet season iHg concentrations. In contrast, the dry seasons (April – September) included two years each of El Niño and La Niña conditions. During the La Niña dry seasons of 2021 and 2022, median iHg concentrations were 23% higher than the El Niño dry seasons of 2023 and 2024 (Mann-Whitney U Test, $p = 4.4 \times 10^{-4}$; Supplementary Fig. 5). We hypothesize that this is due to stronger upwelling during La Niña periods, which transports iHg-rich

waters from depth to the surface[24,25]. While iHg concentrations in deeper waters from the La Jolla Submarine Canyon located near Scripps Pier have not been reported to the best of our knowledge, previous work in the California Current System has identified elevated Hg concentrations in surface waters influenced by upwelling[24,25,40], suggesting that this may be a process that influences surface waters at Scripps Pier. Although our dataset includes only two years each of La Niña and El Niño conditions, limiting the ability to draw definitive conclusions, the observed patterns highlight a potential link between oceanic iHg concentrations and climate indices. Continued monitoring of these processes is essential to validate these trends and improve predictions of iHg variability under future climate scenarios.

Seasonally, surface water iHg concentrations over the course of a year were elevated during the wet season (October to March) and more stable during the dry season (April to September), which is influenced by seasonality of precipitation and wave height (Fig. 2d–f). To better identify and quantify these underlying seasonal trends, we applied singular spectrum analysis. This method uncovered a periodic increase of up to 0.1 pM per month during the wet season, driven by precipitation and wave-induced mixing, followed by decreases during the dry season (Supplementary Fig. 6). Wet season iHg dynamics were influenced by episodic precipitation events, particularly atmospheric rivers, which bring intense winds and multi-day rainfall. These events increase streamflow, urban runoff, and ocean turbulence[41–43], introducing pulses of iHg that cause temporary spikes in concentrations before rapidly returning to baseline levels. This seasonal analysis suggests that precipitation and wave dynamics, which are elevated during the wet season compared to the dry season, exert a strong influence on the system by increasing iHg concentrations.

During the dry season, while concentrations are lower than the wet season due to lower wind speeds and the absence of precipitation events, we find that iHg concentrations positively correlate with wave height measured by buoy LJPC1[44], located within meters of Scripps Pier ($R^2 = 0.165$, $p = 2.5 \times 10^{-7}$, $n = 150$; Supplementary Fig. 7), which reflects wind speed, duration, and fetch[45]. Wave dynamics have a complex influence on iHg concentrations, where turbulent mixing and upwelling can enhance concentrations, while stronger winds driving larger waves can accelerate the evasion of Hg^0, reducing oceanic concentrations. In this study at Scripps Pier, we observed a positive correlation between wave height and iHg concentrations during the dry season, when precipitation is absent. This suggests that while both wave height and iHg concentrations are lower and more stable during the dry season (Fig. 2d, f), increased wave height slightly elevates iHg concentrations. We hypothesize that this relationship is due to upwelling, where wave height can serve as a proxy for mixing and upwelling that enhances iHg concentrations. Upwelling, a known source of iHg to surface waters within California Current System[24,25], brings iHg-rich waters from depth to the surface. To confirm the relationship between wave height and upwelling, we compared the daily average wave height with the modeled Coastal Upwelling Transport Index[46] (CUTI) at 33°N, which is a daily index developed by Jacox et al. to estimate vertical transport of upwelled waters based on the surface wind stress[47]. Higher values of the CUTI represent more water transport due to upwelling, and we find a significant positive correlation between wave height measured by buoy LJPC1 and the modeled CUTI ($R^2 = 0.37$, $p = 7.83 \times 10^{-9}$, $n = 75$; Supplementary Fig. 8). As a result, we use wave height in our analyses as a proxy for upwelling and mixing processes that introduce iHg from depth to surface waters because it is a measured parameter at Scripps Pier.

During upwelling conditions in the dry season, deep La Jolla Submarine Canyon waters that are enriched in nutrients are transported to the surface, stimulating primary productivity[22,28,46,48,49]. The introduction of iHg from upwelled waters[24,25] during these biologically active periods[48] increases its likelihood of undergoing methylation compared to the precipitation-driven inputs of the wet season[9,50,51]. As a result, upwelling-driven iHg inputs may play a critical role in providing substrate for MMHg formation in the water column at Scripps Pier and its subsequent bioaccumulation in marine food webs.

Developing a predictive model for iHg concentrations reveals that physical processes, rather than inputs, drive variability

We aimed to develop a predictive model for oceanic iHg concentrations in this coastal system using measured values from our high-resolution time series and related physical parameters. The first step was to incorporate major inputs, with atmospheric deposition identified as a primary source of iHg. To capture this, we used GEOS-Chem modeled total atmospheric deposition from 2021 to 2023. GEOS-Chem is a global atmospheric chemistry model that estimates wet and dry deposition of iHg by integrating large-scale inputs, such as global anthropogenic emissions, meteorological patterns, and deposition processes[52–54]. We used this model to estimate the monthly mean iHg deposition within the region of 30–40°N and 115–120°W and then searched for correlations between these data and our iHg concentrations on both a weekly and monthly time frame. Our analysis revealed no significant correlations, and this persisted even after incorporating additional physical variables measured at or near Scripps Pier, such as precipitation or wave height. These findings suggest that the GEOS-Chem modeled total atmospheric iHg deposition does not explain the variability in oceanic iHg concentrations observed at this site.

With this result, we investigated alternative drivers of oceanic iHg variability by testing correlations between datasets of local physical processes, such as oceanographic and meteorological measurements, and our measured iHg time series. We iteratively tested various combinations of publicly available datasets of physical factors between 2021 and 2023 through multiple linear regression, such as temperature, salinity, nutrients, and chlorophyll-*a*. Ultimately, we found that streamflow and wave height together explained the largest proportion of iHg variability. The streamflow dataset, provided by the United States Geological Survey, captures weekly average streamflow from the Los Peñasquitos river, with the outflow located 7.5 km north of Scripps Pier[55]. This dataset reflects the cumulative precipitation effects within the watershed, serving as both an indicator of precipitation and terrestrial inputs of iHg to the ocean. On the other hand, the wave height data is a daily average of hourly measurements sourced from buoy LJPC1, located within meters of Scripps Pier[44]. This dataset reflects the impact of coastal hydrodynamic processes that source upwelled water masses, resuspend sediments, and promote mixing. Together, these two factors revealed a significant correlation with measured iHg concentrations that explains 19% of the variability, with 35% of the regression model influenced by streamflow and 44% influenced by wave height ($R^2 = 0.19$, $p = 5.7 \times 10^{-6}$, $n = 116$). Notably, we do not use any iHg concentrations from either of these two sources to develop this model, demonstrating how the magnitude of physical processes alone can be used to predict iHg values. This model, based entirely on physical processes, outperformed attempts to incorporate GEOS-Chem atmospheric deposition data, emphasizing the importance of localized dynamics over large-scale atmospheric inputs in explaining short-term variability.

The distinction in spatial and temporal resolution between GEOS-Chem and localized physical datasets reflects the differences in the processes that they capture. GEOS-Chem provides broad-scale estimates of iHg inputs via atmospheric pathways, which are useful for understanding long-term trends; however, localized datasets are better suited to capture dynamic oceanographic processes, such as upwelling and watershed inputs, that influence how iHg concentrations fluctuate within a local coastal system on a shorter time scale. These processes are inherently linked to the physical datasets of streamflow and wave height, and as a result, we find that they are better suited to explain the variability in iHg concentrations observed in our time series. These results suggest that variability in iHg concentrations on a weekly basis is not primarily determined by total iHg deposition to the system as modeled by GEOS-Chem but rather by how these inputs interact with natural processes controlling iHg cycling and distribution.

To refine our regression model based on streamflow and wave height, we applied an autoregressive moving average component to account for temporal autocorrelation in the residuals (see Supplementary Table 1, Supplementary Fig. 9, and Methods). Figure 3 shows the overall model, which has an $R^2 = 0.82$ ($n = 116$), and was trained with measured iHg

concentrations between 2021 and 2023. To evaluate our model, we compared the model predictions to measurements taken throughout 2024, confirming that the model predicts all but two measured samples within the 99% confidence interval ($n = 47$, Fig. 3, Supplementary Fig. 10). In February 2024, one point falls below the 99% confidence interval due to anomalously high rainfall that does not result in as much of an increase in iHg concentrations in the 0.5 m water sample compared to the 6 m sample (Fig. 2a). The other data point falls above the 99% confidence interval, corresponding to a sharp decline in temperature observed in late September 2024, which we hypothesize reflects the influence of a deeper water mass increasing iHg concentrations (Supplementary Fig. 1a). This temperature decline was not associated with precipitation, and wave height showed only a slight increase (Fig. 2). Since the model is parameterized solely by streamflow and wave height, it could not account for this anomalous iHg concentration. As our time series expands, the model can be improved by incorporating additional parameters, such as temperature or other indicators of water masses. Overall, our results demonstrate that the model reliably reconstructs iHg concentrations on short time scales based on localized physical processes, offering valuable insights into the major drivers of iHg variability in this system. This model highlights the importance of incorporating high-resolution, site-specific datasets in understanding dynamic coastal environments.

Retrospective modeling of iHg concentrations reveals substantial interannual variability driven by natural climate factors

To assess long-term trends due to climate variability, we used our model to reconstruct iHg concentrations in these waters from September 2004 through December 2024 (Fig. 4). The modeled data reveal significant variability in iHg concentrations driven by changes in precipitation and wave height. Based on this data, we detected a long-term decreasing trend of 0.005 pM yr^{-1} over the past 20 years (Mann-Kendall test and Theil-Sen's Slope, $p = 1.0 \times 10^{-5}$). It is important to note that this model does not include source iHg concentrations, which may have varied over the past two decades due to changes in emissions and deposition patterns. As a result, the observed trend cannot be interpreted as an absolute decline in iHg concentrations, but rather it reflects the influence of reductions in natural factors, such as precipitation and wave height, that may have contributed to decreasing iHg concentrations. In California, the past 20 years have been characterized by more dry winters than wet winters (Supplementary Fig. 2), driven in part by the negative mode of the Pacific Decadal Oscillation along with the occurrence of more La Niña conditions (Supplementary Fig. 4)[39,56], which may be causing a decrease in iHg inputs. In the future, climate predictions for California expect increased interannual precipitation variability, and while precipitation events will become less frequent, the intensity of atmospheric rivers is expected to increase[57]. As a result, we hypothesize that the projected reduction in precipitation will decrease iHg inputs to surface waters at Scripps Pier, resulting in a continued decreasing trend in iHg concentrations. However, the major spikes in iHg linked to atmospheric rivers, similar to those observed in 2023 and 2024, will persist. These impacts would be independent of changes in atmospheric deposition due to emissions controls, underscoring the dominant influence of regional hydrological and oceanographic processes at this site. Continuing to monitor oceanic iHg concentrations will allow us to assess the impact of climate change on oceanic iHg, which is an ongoing area of research.

Overall, our time series analysis demonstrates the impact of natural climate variability and ocean processes in influencing iHg concentrations in California's surface waters, both in measured and modeled datasets spanning the past 20 years. While atmospheric deposition affects regional iHg concentrations over longer time scales, our findings highlight shorter-term processes that directly impact oceanic iHg concentrations that may obscure the effects of atmospheric deposition. This work marks the first long-term iHg time series in a marine environment, to the best of our knowledge, and additional global time series are necessary to improve large-scale biogeochemical models and policy assessments. Changes in Hg emissions add an additional layer of complexity in understanding long-term trends, but until we can fully quantify the role of environmental variability in driving oceanic iHg concentrations, it remains challenging to disentangle the effects of emissions reductions from climate-driven changes. Based on these findings, we recommend expanding monitoring programs to create region-specific time series to examine key drivers of Hg variability and to disentangle competing influences from anthropogenic emissions, climate change, and natural variability to ultimately allow for quantifying the timeline for environmental recovery.

Methods

Hg Sampling

Weekly sampling was conducted between December 2020 and December 2024 at Scripps Pier in La Jolla, CA (32.8634 °N, 117.2546 °W; Fig. 1). Total Hg (THg) and total methylated Hg (MeHg: sum of MMHg and dimethylmercury) were sampled at the surface (< 0.5 m depth) and bottom water (6 m depth) using a peristaltic pump equipped with weighted sample tubing. Unfiltered seawater was pumped into clean borosilicate glass bottles (I-Chem) and returned to the lab. MeHg and THg samples were acidified with 0.4% hydrochloric acid (HCl; Trace Metal Grade, J.T. Baker), and stored at 4°C until analysis within 6 months.

Hg Speciation Analysis in Seawater

THg concentrations were measured following U.S. EPA Method 1631e[58,59]. 30 mL samples were amended by bromine monochloride oxidation, hydroxylamine and tin (II) chloride reduction, and purged onto gold traps followed by cold-vapor atomic fluorescence spectrometry (CV-AFS) using a Tekran 2600 Automated Hg Analyzer. Calibration was based on an aqueous 1000 ppm mercuric chloride ($HgCl_2$) standard (SPEX Certiprep®) and confirmed with a second 1000 ppm $HgCl_2$ standard (Alfa Aesar). To validate concentrations, we analyzed the river water certified reference material ORMS-3 (National Research Council Canada, Ottawa, Canada) with a

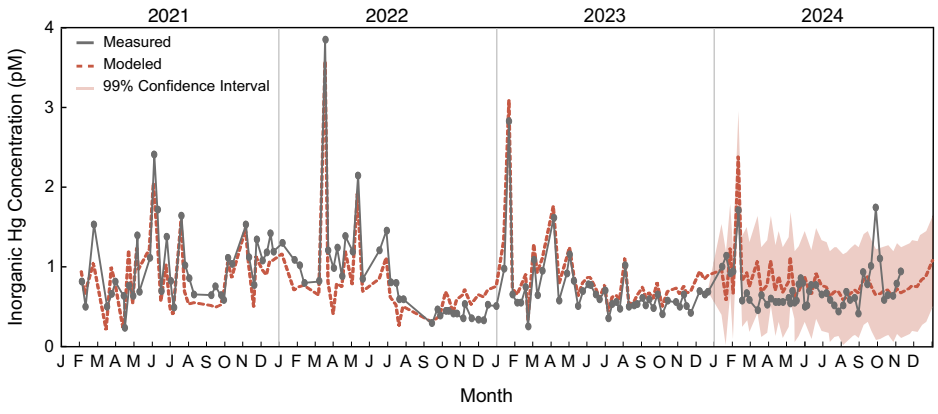

Fig. 3 | Modeled inorganic mercury (Hg) concentrations (red) compared to measured values (gray) at Scripps Pier. The model was constructed using multiple linear regression of streamflow and wave height with an autoregressive moving average component trained with measured iHg concentrations between 2021 and 2023. Modeled data for 2024 is compared to measured data as part of a model validation set. 99% confidence intervals for 2024 modeled data are represented by the shaded region in red.

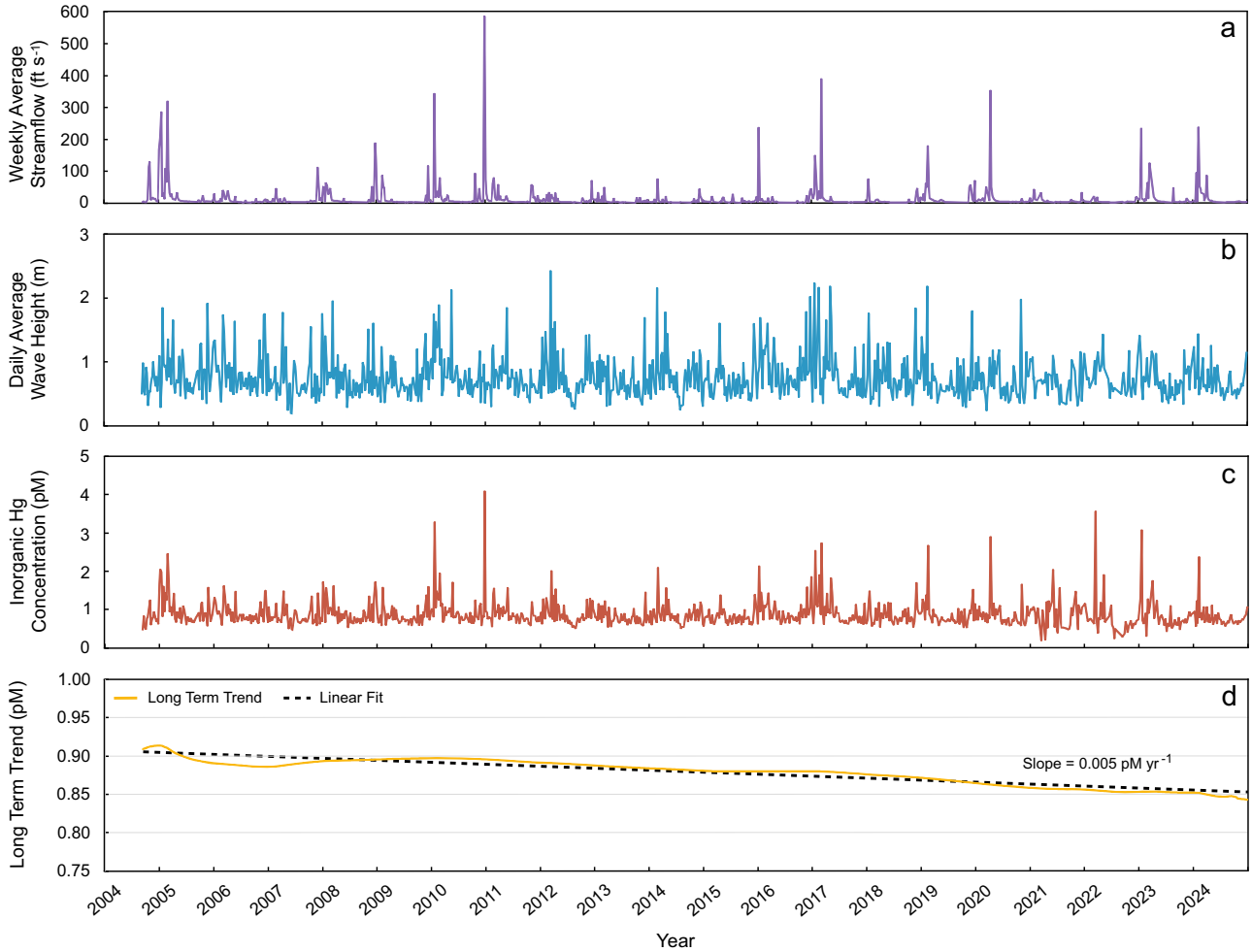

Fig. 4 | Time series from September 2004 to December 2024 for streamflow, wave height, modeled inorganic mercury concentrations, and long-term trend. **a** Weekly average streamflow at Los Peñasquitos river. **b** Daily average wave height from buoy data near Scripps Pier. **c** Modeled concentrations of inorganic mercury (Hg) at Scripps Pier. **d** Long term trend in modeled inorganic Hg concentrations as determined by singular spectrum analysis (solid yellow line) with a linear fit (dashed black line).

certified value of 12.6 ± 1.1 ng L^{-1}[60]. We determined ORMS-3 concentrations to be 14.8 ± 2.44 ng L^{-1} (n = 12). The detection limit was 0.17 pM (n = 75 reagent blanks) with ongoing precision and recovery of 101 ± 6% (n = 73). Average replicate precision was 6% (n = 130), and matrix spike recovery was 93 ± 12% (n = 36).

MeHg samples collected prior to January 2024 were analyzed by ascorbic acid-assisted direct ethylation following Munson et al. (2014) and U.S. EPA Method 1630[61,62]. 45 mL samples were digested overnight with 1% sulfuric acid, then pH-adjusted with potassium hydroxide and acetate buffer. Next, ascorbic acid was added as an antioxidant prior to ethylation with sodium tetraethylborate. Volatile species were preconcentrated onto a Tenax trap, which was then desorbed. Hg species were separated by gas chromatography and quantified via CV-AFS on a Tekran 2700 Automated Methylmercury Analyzer. Calibration curves were based on standards prepared from a certified 1000 ppm aqueous MMHg chloride standard (Alfa Aesar). The detection limit was 0.030 pM (n = 59 reagent blanks), with ongoing precision and recovery of 106 ± 13% (n = 96). Average replicate precision was 7% (n = 195, and matrix spike recovery was 101 ± 25% (n = 69).

Samples taken following January 2024 were quantified via isotope dilution to improve detection. Isotopically enriched monomethyl-^{201}Hg ($MM^{201}Hg$) was synthesized from isotopically enriched inorganic ^{201}Hg (Oak Ridge National Laboratory, TN) for use as an internal standard. Samples were amended by adding the regularly quantified $MM^{201}Hg$ standard at a ratio of roughly 1:1 standard to ambient concentrations[63]. Then acetate buffer was added to the samples, followed by ascorbic acid and ethylation via sodium tetraethylborate. Hg species were then analyzed by a Tekran 2700 coupled to an Agilent 8900 Triple Quadrupole Inductively Coupled Plasma Mass Spectrometer. We defined detection limit as the Hg amount giving a 4.8% signal contribution to the total measured signal intensity at the specific isotope mass as in Jonsson et al.[64] and ensured that samples were above this detection limit. Average replicate precision was 10% (n = 68, and matrix spike recovery was 105 ± 17% (n = 28).

Because MeHg is the sum of all organic Hg species known to exist in measurable concentrations in seawater and THg is a measurement of all Hg species in seawater, iHg concentrations were calculated as iHg = THg – MeHg[4,65].

GEOS-Chem Modeled Atmospheric Hg Deposition

Hg deposition is simulated by a global three-dimensional atmospheric GEOS-Chem Hg model (https: /geoschem.github.io, version 14.4.3). The model has a horizontal resolution of 4° × 5°, with 72 levels vertically. The simulation is driven by the meteorological fields from the NASA Modern-Era Retrospective Analysis for Research and Applications, version 2 system[66]. The primary Hg species in the model are Hg^0, Hg^{II}, and particulate Hg ($Hg^{II}P$). The model simulates the transport, redox, respeciation, photolysis, and deposition of Hg species[52,53]. The global anthropogenic Hg emissions inventory is from Global Mercury Assessment 2018[54], while other emissions are from Horowitz et al., 2017[52]. The redox chemistry mechanism includes the oxidation of Hg^0 by bromide and hydroxide and the subsequent

oxidation of Hg^0 by ozone and radicals to form Hg^{II}[53]. The respeciation between gaseous Hg^{II} and $Hg^{II}P$ occurs when Hg^{II} is absorbed by aerosols or cloud droplets[67]. The global mean photoreduction frequency of organic $Hg^{II}P$ to Hg^0 is 1.9×10^{-5} s^{-1} and is scaled by the local nitrogen dioxide photolysis frequency[53]. In GEOS-Chem, the modeled Hg^{II} and $Hg^{II}P$ undergo both dry and wet deposition, while Hg^0 only undergoes dry deposition because of its low Henry's Law constant. The dry deposition velocity is calculated by a resistance-based scheme, which is affected by meteorological conditions, land type, leaf area index, and features of species[68]. The wet deposition includes the wet scavenging in convective updrafts and washout and rainout in large-scale precipitation. We run the simulation for 2001–2023, with the first years as a spin-up. We use the monthly mean Hg deposition within the region of 30–40°N and 115–120°W for our analysis.

Ancillary Parameters

Temperature, salinity, and biological data, including chlorophyll-*a*, are publicly available through SCCOOS[22,23]. Other parameters, such as nutrient concentrations, are also available on the SCCOOS data portal. Oxygen concentrations are available through the Scripps Ocean Acidification Real-Time Monitoring Program[21] (Supplementary Fig. 1). Precipitation data from Stations US1CASD0030 (La Jolla) and USW00023188 (San Diego International Airport) was accessed via the National Centers for Environmental Information[31], and wave height and wind speed data for Stations LJPC1, 46225, and 46254 were accessed via the National Data Buoy Center[44]. El Niño data from NINO3.4 was accessed from the Physical Sciences Laboratory at the National Oceanic and Atmospheric Administration[69] and the Pacific Decadal Oscillation Index was accessed from the National Centers for Environmental Information[70]. Streamflow data for Los Peñasquitos River Station 11023340 was accessed via the United States Geological Survey[55].

Data Analysis

Time series trend decomposition was performed in MATLAB (Version R2024a). Daily interpolations of iHg concentrations were calculated via the 'retime' function to achieve equal sampling intervals, and the time series was decomposed using Singular Spectrum Analysis with the 'trenddecomp' function.

To develop a multiple linear regression combined with autoregressive moving average model to predict iHg concentrations, the training set consisted of data from January 2021 through December 2023 ($n = 115$). We developed a multiple linear regression model for iHg concentrations with weekly average streamflow data from the Los Peñasquitos River and daily average wave height from station LJAC1 using MATLAB's 'fitlm' function (regression parameters presented in Supplementary Table 1). Then, we applied an autoregressive moving average model to the residuals using the 'arima' function and varying the autoregressive and moving average orders between 0 and 3 to optimize fit. The best model was selected based on the lowest Akaike Information Criterion (AIC) value, ensuring no collinearity among physical parameters and the statistical significance was $p < 0.05$[71]. Residuals were evaluated for mean of 0, normal distribution, and lack of autocorrelation (Supplementary Fig. 9). Final model parameters are presented in Supplementary Table 1. The data collected after January 2024 was used for model validation, with 99% confidence intervals calculated by adding (or subtracting) the z-value multiplied by the Root Mean Squared Error to the forecasted value. Validation statistics are shown in Supplementary Table 1 and a scatter plot comparing model predictions and observed concentration is shown in Supplementary Fig. 10.

For retrospective modeling to 2004, gaps in wave height data for LJPC1 between 2015-2017 were filled using data from the Scripps Nearshore buoy 46254, located approximately 930 m west of LJPC1. Gaps for LJPC1 prior to 2015 were filled using data from the Torrey Pines buoy 46225, located 14.55 km from LJPC1. A linear correlation was applied to buoy 46225 data due to its higher recorded wave height, better aligning it with LJPC1 measurements. Long-term trends for the 20-year modeled dataset were analyzed using the nonparametric Mann-Kendall test, and the annual rate of change was determined by Theil-Sen's slope with the significance level set to $p = 0.05$[72–74].

Data availability

Hg time series data generated from this study is available at the National Science Foundation BCO-DMO repository at https://www.bco-dmo.org/project/908151. Precipitation data from NOAA NCEI is accessible at https://www.ncdc.noaa.gov/cdo-web/datasets/GHCND/stations/GHCND:USW00023188/detail. NINO3.4 is accessible at https://psl.noaa.gov/data/timeseries/monthly/NINO34/. The PDO index is accessible at https://www.ncei.noaa.gov/pub/data/cmb/ersst/v5/index/ersst.v5.pdo.dat. Wave data is accessible at https://www.ndbc.noaa.gov/station_history.php?station=ljpc1. The Coastal Upwelling Transport Index (CUTI) dataset can be accessed at https://mjacox.com/upwelling-indices/. Streamflow data for Los Peñasquitos is accessible at https://waterdata.usgs.gov/monitoring-location/11023340/.

Received: 3 January 2025; Accepted: 28 March 2025;
Published online: 16 April 2025

References

1. Sunderland, E. M. Mercury exposure from domestic and imported estuarine and marine fish in the U.S. seafood market. *Environ. Health Perspect.* **115**, 235–242 (2007).
2. Conaway, C. H., Black, F. J., Weiss-Penzias, P., Gault-Ringold, M. & Flegal, A. R. Mercury speciation in Pacific coastal rainwater, Monterey Bay, California. *Atmos. Environ.* **44**, 1788–1797 (2010).
3. Mason, R. P., Fitzgerald, W. F. & Vandal, G. M. The sources and composition of mercury in Pacific Ocean rain. *J. Atmos. Chem.* **14**, 489–500 (1992).
4. Mason, R. P. et al. Mercury biogeochemical cycling in the ocean and policy implications. *Environ. Res* **119**, 101–117 (2012).
5. Amos, H. M. et al. Global biogeochemical implications of mercury discharges from rivers and sediment burial. *Environ. Sci. Technol.* **48**, 9514–9522 (2014).
6. Mason, R. P., Fitzgerald, W. F. & Morel, F. M. M. The biogeochemical cycling of elemental mercury: Anthropogenic influences. *Geochim Cosmochi m. Acta* **58**, 3191–3198 (1994).
7. Lehnherr, I., St, Louis, V. L., Hintelmann, H. & Kirk, J. L. Methylation of inorganic mercury in polar marine waters. *Nat. Geosci.* **4**, 298–302 (2011).
8. Compeau, G. & Bartha, R. Methylation and demethylation of mercury under controlled redox, pH, and salinity conditions. *Appl Environ. Microbiol* **48**, 1203–1207 (1984).
9. Monperrus, M. et al. Mercury methylation, demethylation and reduction rates in coastal and marine surface waters of the Mediterranean Sea. *Mar. Chem.* **107**, 49–63 (2007).
10. Agather, A. M., Bowman, K. L., Lamborg, C. H. & Hammerschmidt, C. R. Distribution of mercury species in the Western Arctic Ocean (US GEOTRACES GN01). *Mar Chem* **216**, (2019).
11. Bowman, K. L., Hammerschmidt, C. R., Lamborg, C. H. & Swarr, G. Mercury in the North Atlantic Ocean: The U.S. GEOTRACES zonal and meridional sections. *Deep Sea Res 2 Top. Stud. Oceanogr.* **116**, 251–261 (2015).
12. Bowman, K. L., Hammerschmidt, C. R., Lamborg, C. H., Swarr, G. J. & Agather, A. M. Distribution of mercury species across a zonal section of the eastern tropical South Pacific Ocean (U.S. GEOTRACES GP16). *Mar. Chem.* **186**, 156–166 (2016).
13. Bowman, K. L., Lamborg, C. H. & Agather, A. M. A global perspective on mercury cycling in the ocean. *Sci. Total Environ.* **710**, 136166 (2020).
14. Tseng, C. M., Lamborg, C. H. & Hsu, S. C. A unique seasonal pattern in dissolved elemental mercury in the South China Sea, a tropical and monsoon-dominated marginal sea. *Geophys Res Lett.* **40**, 167–172 (2013).

15. Temme, C., Ebinghaus, R., Einax, J. W., Steffen, A. & Schroeder, W. H. Time series analysis of long-term data sets of atmospheric mercury concentrations. *Anal. Bioanal. Chem.* **380**, 493–501 (2004).
16. Zolkos, S. et al. Multidecadal declines in particulate mercury and sediment export from Russian rivers in the pan-Arctic basin. https://doi.org/10.1073/pnas (2022).
17. Eklöf, K. et al. Trends in mercury, lead and cadmium concentrations in 27 European streams and rivers: 2000–2020. *Environ. Pollut.* **360**, 124761 (2024).
18. Zhang, Y. et al. An updated global mercury budget from a coupled atmosphere-land-ocean model: 40% more re-emissions buffer the effect of primary emission reductions. *One Earth* **6**, 316–325 (2023).
19. Schartup, A. T., Soerensen, A. L., Angot, H., Bowman, K. & Selin, N. E. What are the likely changes in mercury concentration in the Arctic atmosphere and ocean under future emissions scenarios?. *Sci. Total Environ.* **836**, 155477 (2022).
20. California Department of Fish and Wildlife. *2023 Marine Region By the Numbers*. (2023).
21. Clements, S. C. et al. Scripps Ocean Acidification Real-time (SOAR) Dataset. *Scripps Institution of Oceanography, La Jolla, CA* (2024).
22. McGowan, J. A. et al. Predicting coastal algal blooms in southern California. *Ecology* **98**, 1419–1433 (2017).
23. Carter, M. L. et al. Shore Stations Program - La Jolla, Scripps Pier (La Jolla Archive, 2024-07-24). In Shore Stations Program Data Archive: Current and Historical Coastal Ocean Temperature and Salinity Measurements from California Stations. *UC San Diego Library Digital Collections* https://doi.org/10.6075/J06T0K0M (2022).
24. Coale, K. H. et al. The distribution and speciation of mercury in the California current: Implications for mercury transport via fog to land. *Deep Sea Res 2 Top. Stud. Oceanogr.* **151**, 77–88 (2018).
25. Adams, H. M., Cui, X., Lamborg, C. H. & Schartup, A. T. Dimethylmercury as a Source of Monomethylmercury in a Highly Productive Upwelling System. *Environ. Sci. Technol.* **58**, 10591–10600 (2024).
26. Mason, R. P., Kim, E. H., Cornwell, J. & Heyes, D. An examination of the factors influencing the flux of mercury, methylmercury and other constituents from estuarine sediment. *Mar. Chem.* **102**, 96–110 (2006).
27. Choe, K. Y. et al. Sediment-water exchange of total mercury and monomethyl mercury in the San Francisco Bay-Delta. *Limnol. Oceanogr.* **49**, 1512–1527 (2004).
28. Hamann, M. M., Alford, M. H., Lucas, A. J., Waterhouse, A. F. & Voet, G. Turbulence Driven by Reflected Internal Tides in a Supercritical Submarine Canyon. *J. Phys. Oceanogr.* **51**, 591–609 (2020).
29. Strode, S. A. et al. Air-sea exchange in the global mercury cycle. *Glob. Biogeochem. Cycles* **21**, GB1017 (2007).
30. Dettinger, M. D., Ralph, F. M., Das, T., Neiman, P. J. & Cayan, D. R. Atmospheric rivers, floods and the water resources of California. *Water ((Basel))* **3**, 445–478 (2011).
31. NOAA National Centers for Environmental Information. Precipitation Data for Station USW00023188.
32. Weiss-Penzias, P. S. et al. Aircraft Measurements of Total Mercury and Monomethyl Mercury in Summertime Marine Stratus Cloudwater from Coastal California. *Usa. Environmentla Sci. Technol.* **52**, 2527–2537 (2018).
33. Weiss-Penzias, P. et al. Total- and monomethyl-mercury and major ions in coastal California fog water: Results from two years of sampling on land and at sea. *Elementa* https://doi.org/10.12952/journal.elementa.000101 (2016).
34. Weiss-Penzias, P. S. et al. Total and monomethyl mercury in fog water from the central California coast. *Geophys Res Lett* **39**, (2012).
35. Li, R. et al. Mercury sources, transport, and transformation in rainfall-runoff processes: Mercury isotope approach. *Water Res* **261**, 122044 (2024).
36. Seelen, E. A., Massey, G. M. & Mason, R. P. Role of Sediment Resuspension on Estuarine Suspended Particulate Mercury Dynamics. *Environ. Sci. Technol.* **52**, 7736–7744 (2018).
37. Checkley, D. M. & Barth, J. A. Patterns and processes in the California Current System. *Prog. Oceanogr.* **83**, 49–64 (2009).
38. Bograd, S. J. & Lynn, R. J. Physical-biological coupling in the California Current during the 1997-99 El Niño-La Niña cycle. *Geophys Res Lett.* **28**, 275–278 (2001).
39. Cayan, D. R., Redmond, K. T. & Riddle, L. G. ENSO and Hydrologic Extremes in the Western United States. *J. Clim.* **12**, 2881–2893 (1999).
40. Conaway, C. H. et al. Dimethylmercury in coastal upwelling waters, Monterey Bay, California. *Environ. Sci. Technol.* **43**, 1305–1309 (2009).
41. Shinoda, T., Zamudio, L., Guo, Y., Metzger, E. J. & Fairall, C. W. Ocean variability and air-sea fluxes produced by atmospheric rivers. *Sci. Rep.* **9**, 2152 (2019).
42. Waliser, D. & Guan, B. Extreme winds and precipitation during landfall of atmospheric rivers. *Nat. Geosci.* **10**, 179–183 (2017).
43. Warrick, J. A. et al. River plume patterns and dynamics within the Southern California Bight. *Cont. Shelf Res* **27**, 2427–2448 (2007).
44. NOAA National Data Buoy Center. Meteorological and oceanographic data collected from the National Data Buoy Center Coastal-Marine Automated Network (C-MAN) and moored (weather) buoys. *NOAA National Centers for Environmental Information. Dataset*. (1971).
45. Thomson, J. & Rogers, W. E. Swell and sea in the emerging Arctic Ocean. *Geophys Res Lett.* **41**, 3136–3140 (2014).
46. Paull, C. K. et al. Anatomy of the La Jolla Submarine Canyon system; offshore southern California. *Mar. Geol.* **335**, 16–34 (2013).
47. Jacox, M. G., Edwards, C. A., Hazen, E. L. & Bograd, S. J. Coastal Upwelling Revisited: Ekman, Bakun, and Improved Upwelling Indices for the U.S. West Coast. *J. Geophys Res Oceans* **123**, 7332–7350 (2018).
48. Nagarkar, M. et al. Temporal dynamics of eukaryotic microbial diversity at a coastal Pacific site. *ISME J.* **12**, 2278–2291 (2018).
49. Kim, H. J., Miller, A. J., McGowan, J. & Carter, M. L. Coastal phytoplankton blooms in the Southern California Bight. *Prog. Oceanogr.* **82**, 137–147 (2009).
50. Munson, K. M., Lamborg, C. H., Boiteau, R. M. & Saito, M. A. Dynamic mercury methylation and demethylation in oligotrophic marine water. *Biogeosciences* **15**, 6451–6460 (2018).
51. Heimbürger, L. E. et al. Methyl mercury distributions in relation to the presence of nano- and picophytoplankton in an oceanic water column (Ligurian Sea, North-western Mediterranean). *Geochim Cosmochim. Acta* **74**, 5549–5559 (2010).
52. Horowitz, H. M. et al. A new mechanism for atmospheric mercury redox chemistry: Implications for the global mercury budget. *Atmos. Chem. Phys.* **17**, 6353–6371 (2017).
53. Shah, V. et al. Improved mechanistic model of the atmospheric redox chemistry of mercury. *Environ. Sci. Technol.* **55**, 14445–14456 (2021).
54. Steenhuisen, F. & Wilson, S. J. Development and application of an updated geospatial distribution model for gridding 2015 global mercury emissions. *Atmos. Environ.* **211**, 138–150 (2019).
55. National Water Information System. *Los Penasquitos C NR Poway CA - 11023340*. https://waterdata.usgs.gov/monitoring-location/11023340/ (2024).
56. Byrne, S. M. et al. Southern California winter precipitation variability reflected in 100-year ocean salinity record. *Commun. Earth Environ.* **4**, 143 (2023).
57. Gershunov, A. et al. Precipitation regime change in Western North America: The role of Atmospheric Rivers. *Sci. Rep.* **9**, 9944 (2019).
58. U.S. Environmental Protection Agency. *Method 1631, Revision E: Mercury in Water by Oxidation, Purge and Trap, and Cold Vapor Atomic Fluorescence Spectrometry Method 1631, Revision E: Mercury in Water by Oxidation, Purge and Trap, and Cold Vapor Atomic Fluorescence Spectrometry Method 1631, Revision E*. (2002).

59. Lamborg, C. H., Hammerschmidt, C. R., Gill, G. A., Mason, R. P. & Gichuki, S. An intercomparison of procedures for the determination of total mercury in seawater and recommendations regarding mercury speciation during GEOTRACES cruises. *Limnol. Oceanogr. Methods* **10**, 90–100 (2012).
60. Yang, L., Willie, S. & Sturgeon, R. E. Ultra-trace determination of mercury in water by cold-vapor generation isotope dilution mass spectrometry. *J. Anal. Spectrom.* **20**, 1226–1231 (2005).
61. U.S. Environmental Protection Agency. *Method 1630: Methyl Mercury in Water by Distillation, Aqueous Ethylation, Purge and Trap, and Cold Vapor Atomic Fluorescence Spectrometry*. (1998).
62. Munson, K. M., Babi, D. & Lamborg, C. H. Determination of monomethylmercury from seawater with ascorbic acid-assisted direct ethylation. *Limnol. Oceanogr. Methods* **12**, 1–9 (2014).
63. Kleindienst, A. et al. Assessing comparability and uncertainty of analytical methods for methylated mercury species in seawater. *Anal. Chim. Acta* **1278**, 341735 (2023).
64. Jonsson, S. et al. Differentiated availability of geochemical mercury pools controls methylmercury levels in estuarine sediment and biota. *Nat. Commun.* **5**, 4624 (2014).
65. Morel, F. M. M., Kraepiel, A. M. L. & Amyot, M. The chemical cycle and bioaccumulation of mercury. *Annu. Rev. Ecol. Syst* vol. 18 www.annualreviews.org. (2025).
66. Gelaro, R. et al. The modern-era retrospective analysis for research and applications, version 2 (MERRA-2). *J. Clim.* **30**, 5419–5454 (2017).
67. Amos, H. M. et al. Gas-particle partitioning of atmospheric Hg(II) and its effect on global mercury deposition. *Atmos. Chem. Phys.* **12**, 591–603 (2012).
68. Feinberg, A., Dlamini, T., Jiskra, M., Shah, V. & Selin, N. E. Evaluating atmospheric mercury (Hg) uptake by vegetation in a chemistry-transport model. *Environ. Sci. Process Impacts* **24**, 1303–1318 (2022).
69. National Oceanic and Atmospheric Administration Physical Sciences Laboratory. Monthly Climate Timeseries: Nino 3.4 SST. https://psl.noaa.gov/data/timeseries/monthly/NINO34/ (2024).
70. National Centers for Environmental Information. Pacific Decadal Oscillation (PDO). *National Oceanographic and Atmospheric Administration*.
71. Burnham, K. P. & Anderson, D. R. *Model Selection and Multimodel Inference: A Practical Information-Theoretic Approach*. (Springer Verlag, New York, 2002).
72. Mann, H. B. Nonparametric Tests Against Trend. *Econometrica* **13**, 245–259 (1945).
73. Hirsch, R. M., Slack, J. R. & Smith, R. A. Techniques of trend analysis for monthly water quality data. *Water Resour. Res* **18**, 107–121 (1982).
74. Yue, S., Pilon, P. & Cavadias, G. *Power of the Mann±Kendall and Spearman's Rho Tests for Detecting Monotonic Trends in Hydrological Series*. www.elsevier.com/locate/jhydrol.
75. Dong, C., Idica, E. Y. & McWilliams, J. C. Circulation and multiple-scale variability in the Southern California Bight. *Prog. Oceanogr.* **82**, 168–190 (2009).
76. Di Lorenzo, E. Seasonal dynamics of the surface circulation in the Southern California Current System. *Deep Sea Res 2 Top. Stud. Oceanogr.* **50**, 2371–2388 (2003).

Acknowledgements

We acknowledge the U.S. National Science Foundation (grant #OCE-2023046 to A.T.S.) and the Simons Foundation (grant #922897 to A.T.S.) that supported the collection, analysis, and writing of this current work. We thank all of the data collectors and managers involved in the SCCOOS and SOAR datasets, along with C. McDonald and R. Walsh for managing research off Scripps Pier. Many have been involved in sampling over the years, and we thank E. Paulson, C. Sephus, A. Carrick-Gonzales, A. Hernandez, and E. Ling for their assistance. We thank E. Paulson, K. Barbeau, and J. Figueroa for their review and feedback to this work.

Author contributions

A.T.S. and C.H.L. conceived of the study and obtained funding. H.M.A. led the sample collection and analysis, and I.K.D. assisted with sample collection and analysis. J.S.B. provided sampling equipment. H.M.A. analyzed and interpreted the data with input from A.T.S., C.H.L., J.S.B. P.W. provided GEOS-Chem model output and interpretation. H.M.A. and A.T.S. wrote the manuscript with contributions from P.W., and all coauthors provided feedback throughout the writing process.

Competing interests

The authors declare no competing interests.

Additional information

Supplementary information The online version contains supplementary material available at https://doi.org/10.1038/s43247-025-02263-8.

Correspondence and requests for materials should be addressed to Hannah M. Adams or Amina T. Schartup.

Peer review information *Communications Earth & Environment* thanks Mengli Chen and the other, anonymous, reviewer(s) for their contribution to the peer review of this work. Primary Handling Editors: Adam Switzer, Somaparna Ghosh.